Geophysical Research Letters

RESEARCH LETTER
10.1029/2021GL097261

Concentrated and Intensifying Humid Heat Extremes in the IPCC AR6 Regions

Simone Speizer[1], Colin Raymond[2], Catherine Ivanovich[3], and Radley M. Horton[4]

[1]Southern Climate Impacts Planning Program, University of Oklahoma, Norman, OK, USA, [2]Jet Propulsion Laboratory/California Institute of Technology, Pasadena, CA, USA, [3]Department of Earth and Environmental Sciences, Columbia University, New York, NY, USA, [4]Lamont-Doherty Earth Observatory, Columbia University, New York, NY, USA

Key Points:

- From 1979 to 2019, extreme wet-bulb temperatures intensified in most IPCC AR6 regions, though to varying degrees
- Patterns in interannual clustering of extreme humid heat show signals of the overall warming trend and the El Niño-Southern Oscillation
- In some arid regions, extreme humid heat days often occur in close temporal proximity to one another and to precipitation events

Supporting Information:

Supporting Information may be found in the online version of this article.

Correspondence to:

S. Speizer,
simone.speizer@gmail.com

Citation:

Speizer, S., Raymond, C., Ivanovich, C., & Horton, R. M. (2022). Concentrated and intensifying humid heat extremes in the IPCC AR6 regions. *Geophysical Research Letters*, *49*, e2021GL097261. https://doi.org/10.1029/2021GL097261

Received 2 DEC 2021
Accepted 19 FEB 2022

Abstract Extreme humid heat events have seen rapid increases globally in recent decades, but regional changes and higher-order temporal characteristics, such as interannual and intra-annual clustering, have not been widely explored. Using ERA5 reanalysis data from 1979 to 2019, we find increasing trends of varying magnitudes in extreme wet-bulb temperatures at the Intergovernmental Panel on Climate Change Sixth Assessment Report (IPCC AR6) regional scale. In many locations, interannual variations in extremes show a strong relationship with the El Niño-Southern Oscillation. The temporal proximity of precipitation events to humid heat days in arid regions suggests that local moisture effects may lead to clustering. Knowledge of these spatial and temporal patterns aids in understanding how potential heat stress is increasing, as well as facilitates the development of regionally specific adaptation and mitigation strategies for combating the associated societal impacts.

Plain Language Summary Extreme humid heat, or the combination of high temperature and humidity, poses a more severe threat to human health than does dry heat alone. Though extremes are particularly dangerous, even moderate levels of humid heat can lead to a variety of health and socioeconomic effects. Motivated by the growing demand for regional, decision-relevant climate information, we calculate historical changes in the intensity of humid heat extremes in the regions used in the Intergovernmental Panel on Climate Change Sixth Assessment Report. Humid heat extremes have intensified in most regions, though some areas have experienced greater increases than others. The timing of extremes also affects their impacts, and thus we additionally analyze how humid heat extremes are distributed, both within the year and across all years. In many locations across the world, extreme humid heat is more common during strong El Niño episodes. In some typically dry regions, extremes tend to occur near each other within a given year and around the same time as rainfall events. Our results help advance the understanding of potential heat stress and the development of regionally specific strategies for combating its impacts.

1. Introduction

Extreme heat can have substantial consequences for human health, especially when paired with humidity (Buzan & Huber, 2020; Di Napoli et al., 2019; Foster et al., 2021). The majority of heat dissipation necessary for human thermoregulation occurs through evaporative cooling via sweating (Gagnon & Crandall, 2018), rendering extreme humid heat more physiologically stressful than extreme temperature alone (Vanos & Grundstein, 2020). Humid heat extremes are rapidly increasing in frequency (Raymond et al., 2020; Rogers et al., 2021), and are projected to continue to intensify in the warming climate (Coffel et al., 2018), significantly increasing exposure to dangerous levels of humid heat.

Various indices are used to quantify the combined impact of temperature and humidity. Wet-bulb temperature (TW) is a particularly useful metric, as it establishes a maximum tolerable intensity of humid heat at about 35°C (Sherwood & Huber, 2010). This survivability limit applies to healthy individuals under optimal external conditions (e.g., in full shade, with access to unlimited drinking water) (Raymond et al., 2020; Sherwood & Huber, 2010). Thus, substantial health effects—including mortality—occur at far lower TW values (Buzan & Huber, 2020; Raymond et al., 2020; Vecellio et al., 2022). Even less extreme magnitudes of humid heat can cause a variety of societal impacts, such as decreased economic productivity associated with limitations on outdoor labor or increased energy demand due to the need for artificial cooling (e.g., Borg et al., 2021; Dunne et al., 2013; Kjellstrom et al., 2016; Sathaye et al., 2013; Zander et al., 2015).

Recent studies examined historical trends in TW extremes in the global aggregate (Raymond et al., 2020), across the world (Rogers et al., 2021), and in specific countries or small regions (e.g., Freychet et al., 2020; Mishra et al., 2020; X.-X. Li, 2020). However, a globally comprehensive assessment of regional changes in extreme TW values has not been conducted. Such an analysis is particularly warranted given the current research emphasis on providing climate information that is useful for regional risk assessment and decision-making (Chen et al., 2021). Though previous work evaluated regional trends in other humid heat metrics, such as wet-bulb globe temperature, those studies only considered a limited set of regions, none of which were in Africa or South America (C. Li, et al., 2017; Willett & Sherwood, 2012). Extending those analyses, we use ERA5 reanalysis data to calculate trends in the intensity of extreme TW values for the land regions in the IPCC AR6 report (Iturbide et al., 2020). These regional-level results complement prior global-scale analyses and more process-oriented work (e.g., Freychet et al., 2020; Mishra et al., 2020; Rogers et al., 2021).

While trends are important for assessing medium- and long-term risks, the timing of extreme events also affects their impacts in a variety of essential ways. For example, subseasonal temporal compounding influences health outcomes and societal response capacity (Baldwin et al., 2019; Margolis, 2014; Spangler & Wellenius, 2021). Additionally, risks vary substantially between locations, with those that rarely see heat stress most strongly affected when it does occur (Guirguis et al., 2018). We conduct a novel assessment of clustering of extreme TW values across the globe, both across and within years, and consider processes (such as precipitation) relevant to particular identified hotspots. Information about interannual and intra-annual clustering can help inform planning and management strategies, over both long- and short-term timescales, by sectors that are particularly vulnerable to the effects of extreme humid heat, such as agriculture, public health, and energy. This analysis also serves as a step toward better understanding the drivers of extreme humid heat and characterizing its impacts in the places where these are most severe.

2. Materials and Methods

2.1. Data

We use ERA5 hourly gridded data ($0.25° \times 0.25°$) from 1979 to 2019 (Copernicus Climate Change Service, 2017). We calculate TW from dry-bulb temperature, dew point temperature, and surface pressure, using code adapted from Kopp (2020) to perform the Buzan et al. (2015) implementation of the Davies-Jones formula for TW (Davies-Jones, 2008). The Buzan method is preferred, particularly for assessments of extremes, as it produces less error at high temperatures than other formulas (Buzan et al., 2015). We obtain the daily maximum TW as the maximum of the hourly values. For precipitation, we sum hourly total accumulation data to calculate daily total precipitation. To quantify the El Niño-Southern Oscillation (ENSO), we use the December–February (DJF) value of the Oceanic Niño Index (ONI) (NOAA, 2021).

2.2. Trends

For each grid cell, we define the extreme and median TW values for each year as the 99th and 50th percentiles, respectively, of the daily maximum TW values in that grid cell and year. We average the extreme and median values for each year over the 46 land regions in the AR6 WGI Reference Set of Land and Ocean Regions (Iturbide et al., 2020). Only land grid cells are included in each regional average, and each grid cell's value is weighted by the cosine of its latitude. We calculate linear trends over 1979–2019 using an ordinary least squares regression, assessing significance with a *t*-test on the slope coefficient.

2.3. Clustering

For each grid cell, we calculate the overall 99th percentile daily maximum TW, drawn from the full 41-year historical data set. We then define extreme wet-bulb days as those with maximum TW values equal to or above this threshold. To examine their spread across the years, we obtain the number of extreme wet-bulb days per year, rank the years in descending order, and calculate the number of years needed to cumulatively reach at least 75% of the total extreme wet-bulb days. We analyze the intra-annual clustering of extremes by computing the "extreme wet-bulb concentration" (EWC), which we define as the average number of extreme wet-bulb days in a two-week window surrounding each extreme day (window begins/ends 1 week before/after each extreme day,

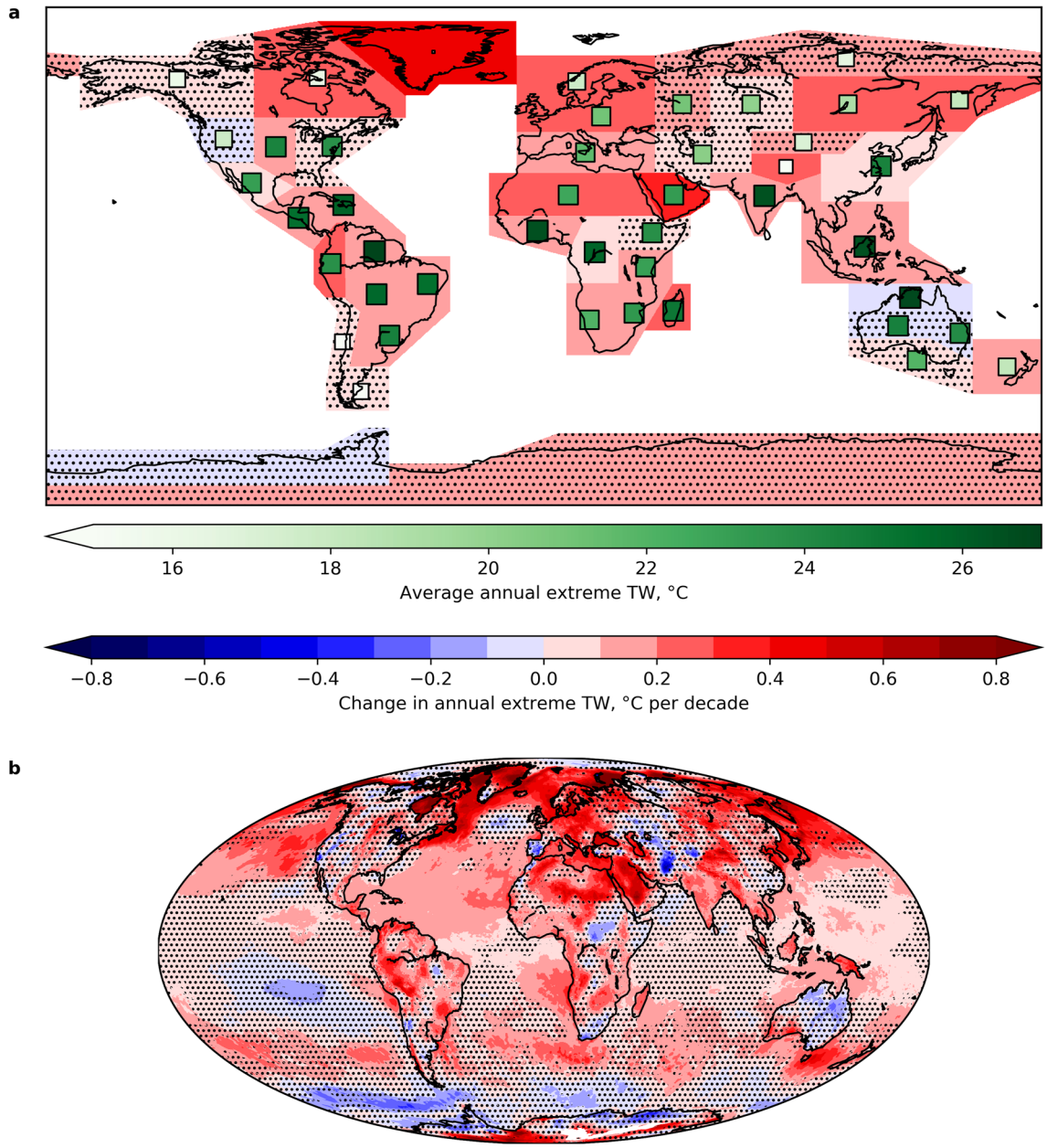

Figure 1. (a) Linear trends in regional averages of the annual extreme (99th percentile) wet-bulb temperature for the Sixth Assessment Report land regions, 1979–2019. Regional averages only include land grid cells, with each grid cell's value weighted by the cosine of its latitude. Shading indicates the coefficient (in °C per decade) of the trend. Stippling indicates where trends are not statistically significant at the 0.05 level. Squares in each region show the average of the annual regionally averaged 99th percentile values; larger and darker green squares indicate higher average values. Only positive averages are shown, and averages below 15°C appear in white. (b) Linear trends as in (a) but computed at a grid cell level.

with a minimum possible EWC value of one). In calculating global statistics, we again weight each grid cell by the cosine of its latitude.

3. Results

We find increasing trends in extreme TW values in most of the AR6 land regions (Figure 1a, Table S1 in Supporting Information S1). Only one region—North Australia—has a statistically significant decreasing trend in extreme TW values; this region has also been highlighted in previous work (Willett & Sherwood, 2012).

Approximately half of the regions have statistically significant trends that correspond to an increase of more than 0.5°C in extreme TW from 1979 to 2019. These rapidly warming regions include four of the top five when ranked by average annual extreme TW: Northern South America, West Africa, South Asia, and Southeast Asia (Figure 1a) (Table S2 in Supporting Information S1). In all four, multiple years in the last decade have seen regionally averaged extreme TW values exceeding 27°C, a threshold considered dangerously hot and humid (Krakauer et al., 2020).

Extreme TW values are warming more rapidly than median conditions in all AR6 regions in Central America, South America, and Africa (except West Africa), as well as in the Arabian Peninsula (Figure S2a in Supporting Information S1). In contrast, in all North American, Asian, European, and Australian regions, extremes are increasing at a slower rate than the median. Most of the regions with the largest trends in median TW values are in the Northern Hemisphere mid or high latitudes (Figure S1a in Supporting Information S1), while relatively large trends in extremes are more commonly found in the tropics and subtropics (Figure 1a).

The regional trends are generally consistent with those computed at the grid cell level, though the spatial smoothing results in trends of smaller magnitude (Figure 1b) (Figure S1b in Supporting Information S1). The grid cell level analysis also identifies small-scale hotspots of extreme TW intensification. For example, portions of the Arabian Peninsula, western China, the Sahara Desert, central Europe, the eastern foothills of the Andes mountains, and some polar regions have trends that equate to an increase of more than 2°C in extreme TW over 1979–2019 (compared with a 0.44°C increase in the global mean extreme TW over this period). Many of these regions also appear in Buzan and Huber (2020), and have experienced particularly large increases in extreme humid heat frequency (Rogers et al., 2021). Locations along the Persian Gulf and parts of the lowlands abutting the Andes are especially noteworthy because they already have overall 99th percentile values greater than 27°C. The grid cell level results also indicate that there are a few isolated land areas with statistically significant decreasing trends in extreme TW values, most notably in Afghanistan and northeastern Australia.

While trends broadly highlight the changing risks of extreme humid heat, societal impacts also depend on the temporal distribution. This concept can be defined in various ways; in Figure 2a, we consider the peak wet-bulb year (year with the highest number of extreme wet-bulb days) at each grid cell. Certain years appear frequently and in coherent regions, with 1998 being the most common (14.4% of all grid cells). The other most prevalent years are 2016 (10.9%), 2019 (10.2%), 2010 (7.1%), 2015 (5.2%), and 1983 (4.8%), versus 2.4% as would be expected by chance (100% divided by 41 years). Combined, this set of years suggests substantial influences of both the global-warming trend and the El Niño-Southern Oscillation (ENSO). The three strongest El Niño episodes since 1979 were 2015–2016, 1997–1998, and 1982–1983 (NOAA, 2021), and for more than a quarter of the grid cells, particularly in the tropics, 1998, 2016, or 1983 is the peak wet-bulb year. When only considering land grid cells, the ENSO influence is somewhat less pronounced: 1998 occurs most frequently (10.9% of the land grid cells), followed by 2010 (10.6%), 2016 (8.8%), 2019 (7.3%), and 2018 (5.1%). These 5 years also had high levels of annually averaged land and population exposure to extreme humid heat (Rogers et al., 2021). Additionally, distinct differences between the ocean and land exist at many coastlines in Figure 2a. For example, 2019 is the peak wet-bulb year along much of the coastlines of eastern India and western Africa, but other years (e.g., 1998) tend to appear in the adjacent oceans.

To obtain a broader sense of the extent to which humid heat extremes cluster in particular years, we also compute the number of years needed to reach at least 75% of the total extreme wet-bulb days (Figure 2b). Years are added in descending rank order, beginning with the top year as shown in Figure 2a; in the hypothetical case of an equal number of extreme days in each year, 31 years would be required to reach 75%. We find that the highest number of years needed across the world is 24 and the lowest is just two. Nearly three quarters (70.7%) of the grid cells require less than 15 years to reach 75% of the days, though when considering only land grid cells this percentage drops to 38.9%. The ENSO influence also appears in this assessment of interannual clustering: worldwide, extreme wet-bulb days are more than twice as common during very strong El Niño years (DJF ONI > 2) than during ENSO-neutral years (DJF ONI between -0.5 and 0.5), and more than three times as common than during moderate to strong La Niña years (DJF ONI between -2 and -1) (Figure S3 in Supporting Information S1). Many tropical regions have strong positive correlations between the annual number of extreme wet-bulb days and the DJF ONI (Figure S4 in Supporting Information S1) as well as relatively high levels of interannual clustering (Figure 2b).

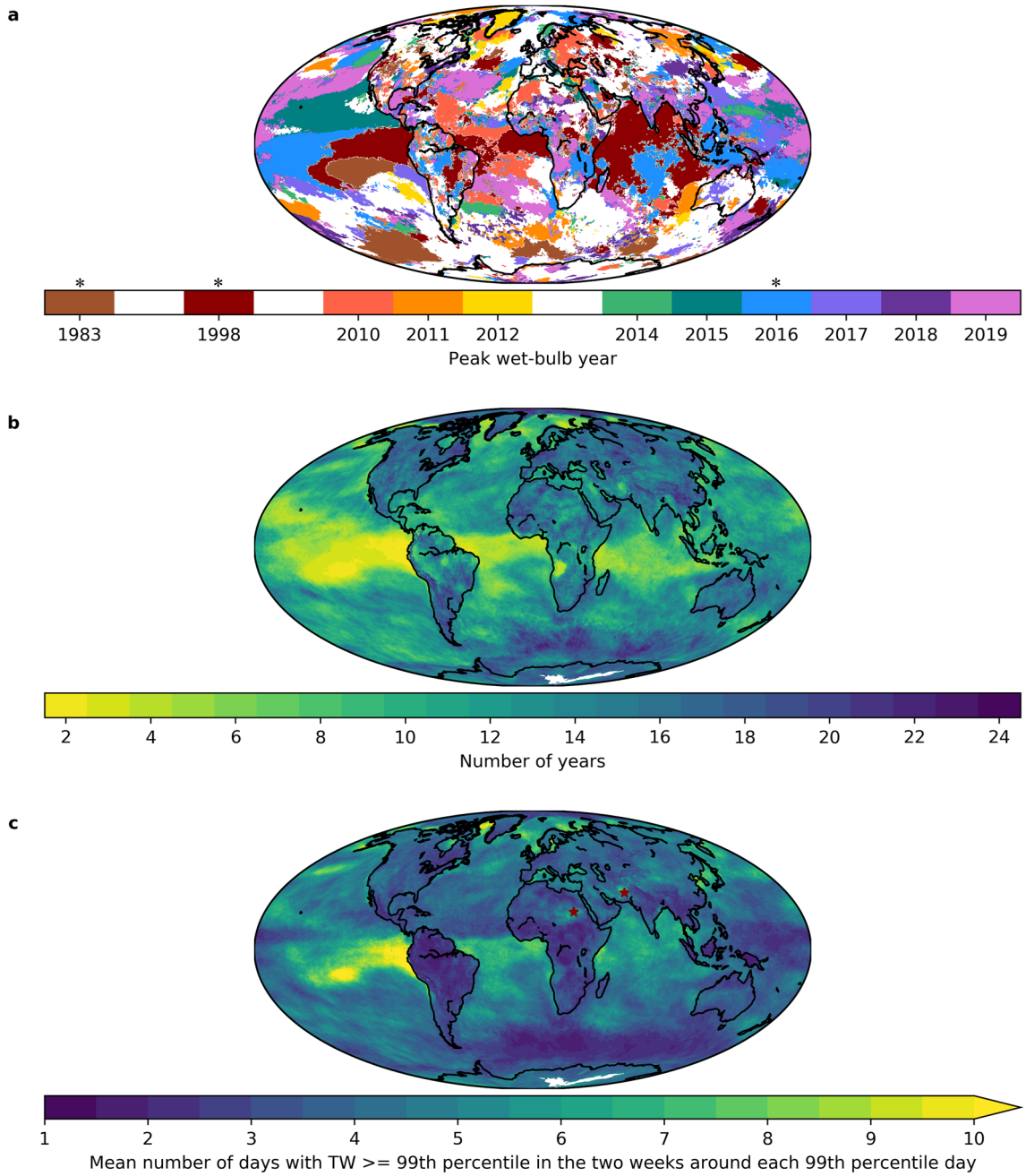

Figure 2. (a) Peak wet-bulb year: the year with the highest number of days at or above the overall 99th percentile wet-bulb temperature (TW) (calculated locally using the full time series of 1979–2019). Only years that cover more than 2% of the globe are shown. Asterisks in the legend indicate very strong El Niño years. If 2 years tie for the same maximum number of days, the earlier year is shown. (b) Number of years needed to cumulatively reach at least 75% of the total days at or above the overall 99th percentile TW. (c) Extreme wet-bulb concentration (EWC): average number of days with TW at or above the overall 99th percentile in a two-week window around each 99th percentile day. Dark red stars indicate the two EWC hotspots analyzed in Figures 3a–3d.

As a springboard for investigations of the processes and risks associated with extreme TW temporal clustering, we next examine autocorrelation over two-week intervals (Figure 2c). The mean extreme wet-bulb concentration (EWC) across all grid cells is 4.1 days (3.4 days over land only), indicating that each extreme wet-bulb day is typically accompanied by several others within 1 week before or after. The consistent climate of the tropical rainforests in much of northern South America, central Africa, Central America, and Southeast Asia is associated with little day-to-day clustering (EWC less than 2.75); in these regions, wet-bulb extremes can happen at any time of year (Rogers et al., 2021). In contrast, most locations with substantial daily clustering (EWC greater than 5) are in

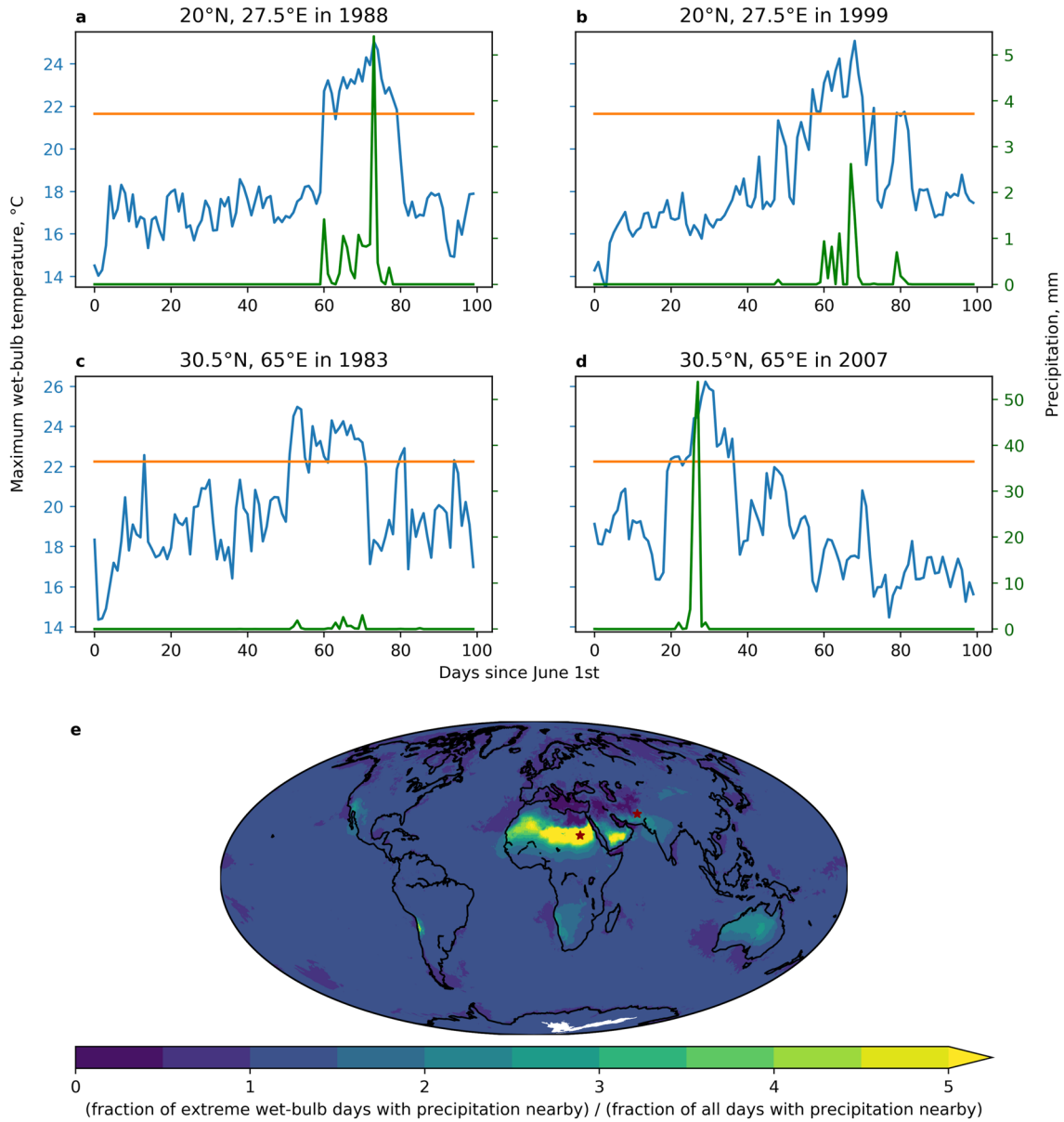

Figure 3. (a)–(d) Time series of daily maximum wet-bulb temperature (TW) (blue) and total precipitation (green) for the locations marked with stars in Figure 2c: (a), (b) 20°N, 27.5°E and (c), (d) 30.5°N, 65°E. Data are shown for the years with the highest (left) and second-highest (right) number of 99th percentile TW days at each location. Time series begin on June 1st of each year and include 100 days. The orange horizontal line indicates the overall 99th percentile daily maximum TW. Wet-bulb and precipitation axes scales are consistent for each location (across rows), but vary between locations. (e) The fraction of 99th percentile TW days that have precipitation in the day before, same day, and/or day after, relative to the fraction of all days that have precipitation in the day before, same day, and/or day after, for each grid cell. Data span 1979–2019. Dark red stars indicate the locations analyzed in (a)–(d).

desert areas: northeastern Africa, the northern and eastern sections of the Persian Gulf, the Pacific coast of South America, and portions of Turkey, Afghanistan, northern China and Mongolia, and the western United States.

Given that many EWC hotspots are located in arid regions, we consider whether an influx of anomalous moisture associated with precipitation events may be linked to the identified clustering of extreme wet-bulb days. Indeed, extreme TW values tend to occur in close temporal proximity to precipitation events in two desert locations with high EWC: northern Sudan and southern Afghanistan (Figures 3a–3d). Figures 3a–3d show time series of daily maximum TW and total precipitation for a representative grid cell from these regions, presenting data from the years with the highest and second-highest number of extreme wet-bulb days at each grid cell. In both locations and years sampled, there is a period of 10–20 days that has extreme TW values on most days as well as multiple

precipitation events. Extending this exploration to a global scale, we consider the likelihood of precipitation in close temporal proximity to extreme wet-bulb days at each grid cell (Figure 3e). In certain areas, extreme wet-bulb days are far more likely than normal to have precipitation in the surrounding days; most of these regions are located in deserts and also have high levels of extreme wet-bulb daily clustering (Figure 2c). These exploratory results hint at how high TW values in dry regions may occur due to some combination of moisture advection, previously shown to be important in arid coastal areas (Monteiro & Caballero, 2019; Pal & Eltahir, 2016), and surface evaporation.

4. Discussion

Our findings of warming extreme TW values in many of the AR6 regions extend previous results indicating increases in humid heat extremes across the world (Raymond et al., 2020; Rogers et al., 2021) and in parts of Asia, Europe, and North America (C. Li, et al., 2017; Freychet et al., 2020; Mishra et al., 2020; X.-X. Li, 2020). They also contrast with the results of studies considering only changes in dry-bulb extremes (Thiery et al., 2020). Of the four AR6 regions with both high extreme TW baselines and comparatively large trends, three are heavily populated and relatively resource-limited (West Africa, South Asia, and Southeast Asia).

In many regions there are close similarities between trends in dry- and wet-bulb extremes (Rogers et al., 2021). Regions with differences, however, are notable and motivate an exploration of potential drivers. Previous studies have suggested that humidity can be important, especially for arid regions, through moisture advection and/or soil moisture effects due to either irrigation or precipitation (Kang & Eltahir, 2018; Krakauer et al., 2020; Liu et al., 2019; Mishra et al., 2020; Monteiro & Caballero, 2019; Pal & Eltahir, 2016). Our results corroborate this hypothesis and provide fresh evidence for it. Figure 3 suggests that strings of high TW days in arid regions may occur due to pulses of moisture that linger for several days, with the atmospheric component amplified by soil moisture feedback. Precipitation events occur before, coincident with, and after extreme wet-bulb days, with coincidence most common both worldwide and specifically in many arid regions (Figure S5 in Supporting Information S1). These initial explorations, though preliminary and limited by their lack of consideration of autocorrelation and other nuances, motivate future investigations of the connection between extreme humid heat, moisture, and precipitation.

Similar humidity effects can also explain many of the most notable trends in extreme humid heat intensity (Figure 1). First, we observe large positive trends in extreme TW values in the Arabian Peninsula, which has experienced substantial increases in irrigation and dew point temperatures since the early 1980s (Lo et al., 2021; Odnoletkova & Patzek, 2021). A similar mechanism may be operating in the opposite sense in Afghanistan, where the area irrigated decreased by about 50% between 1980 and the early 2000s (United Nations Assistance Mission in Afghanistan, 2016). Evapotranspiration there has decreased commensurately (Jung et al., 2010), suggesting that the reduction in irrigation may partially account for the large declines in extreme TW (Figure 1b). Other regions where observed humidity decreases may help explain negative extreme TW trends include northern Australia, the western US, Spain, and central Africa (Figure 1) (Gulev et al., 2021; Vicente-Serrano et al., 2018; Willett & Sherwood, 2012).

We further propose that moisture variations are relevant to interannual patterns of humid heat. Levels of interannual clustering of extreme wet-bulb days are high along many coastlines relative to other land areas (Figure 2b). In arid coastal regions, high TW values often occur when marine air masses move onshore (Pal & Eltahir, 2016), and thus fluctuations in sea surface temperatures (SSTs), which tend to be relatively persistent, may play a role in promoting clustering. SST variability—and its associated impacts on atmospheric temperature and humidity—may also partially account for the substantial clustering that we observe near strong ocean currents, such as the equatorial currents, the Gulf Stream, and the eastern boundary currents of Africa and the Americas (Figures 2b and 2c).

Though local-to-regional moisture effects are important in some locations, global-scale temperature and circulation anomalies appear to be the principal drivers of interannual variability and clustering of extreme TW values. Our results especially emphasize the influence of ENSO (Figure 2a and Figures S3 and S4 in Supporting Information S1). Many ocean regions with high interannual clustering also experienced peak wet-bulb years during strong El Niño episodes (Figures 2a and 2b) and show strong relationships between ENSO and the annual number of extreme wet-bulb days (Figure S4 in Supporting Information S1). On land, we observe El Niño-driven humid

heat in many regions that typically exhibit positive dry-bulb temperature anomalies during El Niño, including northern and central South America, central and southern Africa, northwestern North America, and Southeast Asia (Figure 2a and Figure S4 in Supporting Information S1) (Rogers et al., 2021; WMO, 2020), agreeing with previous findings (Raymond et al., 2020; Rogers et al., 2021; X.-X. Li, 2020). However, we also find connections between ENSO and extreme humid heat in regions that less commonly display an El Niño signature in dry-bulb temperature, including parts of western Asia and western and central North America (Figure 2a and Figure S4 in Supporting Information S1). Some of these areas tend to experience more precipitation during El Niño years (WMO, 2020), suggesting that, to the extent that total precipitation and count of wet days are correlated, elevated humidity levels may contribute to the increased frequency of wet-bulb extremes in these years. Further research is necessary to investigate this hypothesis and more rigorously explore the effect of ENSO on extreme humid heat.

Our analyses also highlight the role of long-term warming in shaping year-to-year variations in TW extremes. High levels of interannual clustering are often coincident with relatively large positive trends in extreme humid heat intensity (Figures 1 and 2b), suggesting that the clustering in these regions partly reflects shifting distributions with anthropogenic warming. In parts of Angola, a hotspot of interannual clustering (Figure 2b), nearly all extreme TW days occurred in the last 5 years. Much of southern Angola has been in moderate to severe drought since 2014 (Limones et al., 2020), and thus land-atmosphere feedbacks related to the dry surface may have driven such a large temperature increase that TW values also reached new peaks. Additionally, excepting the El Niño-driven years of 1983 and 1998, all of the globally most common peak wet-bulb years are from the last decade (Figure 2a). While previous analyses and media reports of recent heat extremes drew attention to the Northern Hemisphere midlatitudes, the regions that set extreme wet-bulb exceedance records in 2017, 2018, or 2019 are instead concentrated in eastern and southern Asia and northern and central Africa. This discrepancy points to a lack of awareness of cumulative humid heat extremes and their potential effects, particularly in tropical and subtropical regions sometimes characterized by relatively high vulnerability.

5. Conclusion

In analyzing trends and temporal concentration of extreme TW values, we find notable spatial variations that provide insight into the mechanisms and potential impacts associated with extreme humid heat. Variations in trends appear both at the grid cell level and when aggregated to IPCC AR6 regions, and are likely driven by a combination of warming temperatures in most locations and regionalized drying or moistening trends. As a result, a large majority of the world experienced its peak wet-bulb year since 2010. ENSO is responsible for a significant fraction of wet-bulb extremes over oceans and relatedly the concentration of extremes into a few years. On intraseasonal timescales, clustering is most pronounced as a consequence of arid regions' sensitivity to moisture; there, many extreme wet-bulb days occur in close temporal proximity and in relation to precipitation events.

Though we propose potential drivers of the identified trends and clustering, more research is needed to better understand both the causes of global variability and the processes relevant on a local level. Our analysis of precipitation and TW extremes preliminarily explores one such process, motivating a more comprehensive examination of the connection between rainfall and humid heat over broader temporal and spatial scales. Reanalysis data resolution limits the accuracy and representativeness of our work on finer geographic scales, emphasizing the need for higher resolution observational datasets, particularly those that can be used for accurate coupled model experiments. Similarly, the expansion and validation of long-term irrigation datasets would facilitate additional research on soil moisture feedbacks and extreme humid heat, which would complement further analyses of the relative contributions of changes in dry-bulb temperatures and relative humidity to the wet-bulb trends that we observe. Potential inhomogeneities in the ERA5 relative humidity data set may affect our calculations of trends and interannual variability (Schröder et al., 2019), contributing to uncertainties that additional research could quantify. Future work could also more thoroughly examine the prevalence, patterns, and societal effects of clustered TW extremes. Studies on the cumulative health and economic impacts of temporally compound humid heat would extend previous analyses of noncompound events (e.g., Dunne et al., 2013; Goldie et al., 2017; Mora et al., 2017) and compound dry heat (Baldwin et al., 2019), further illuminating the implications of the clustering we observe.

By highlighting large-scale areas of exposure, our results can help inform decision-making about humid heat mitigation and adaptation, supporting the regionally focused elements of the IPCC AR6 report (Ranasinghe et al., 2021). Our analyses of interannual and daily clustering provide complementary information for

understanding and preparing for the impacts of extreme humid heat. In regions where day-to-day clustering is common, it may be beneficial to maintain heat mitigation or avoidance strategies beyond the first occurrence of a humid heat extreme, as more extremes are likely to follow shortly. Information about the interannual concentration of extremes can be useful for longer-term planning. For example, locations with high levels of interannual clustering may have years with significantly more humid heat exposure than usual. Taking into account these possible outlier years can help inform robust preparedness efforts across domains such as public health and energy supply.

Conflict of Interest

The authors declare no conflicts of interest relevant to this study.

Data Availability Statement

Hourly ERA5 reanalysis data are available at https://cds.climate.copernicus.eu/cdsapp#!/dataset/reanalysis-era5-single-levels?tab=form. ONI data are available at https://origin.cpc.ncep.noaa.gov/products/analysis_monitoring/ensostuff/ONI_v5.php. Code used to calculate wet-bulb temperature was provided by Bob Kopp and is available at https://github.com/bobkopp/WetBulb.m. Code used to conduct the analyses and produce the figures is available at https://github.com/sspeizer/speizeretal_2022_humidheatextremes.

Acknowledgments
Funding for Simone Speizer, Catherine Ivanovich, and Radley M. Horton was provided by the National Oceanic and Atmospheric Administration's Regional Integrated Sciences and Assessments Program, grants NA18OAR4310337 (Simone Speizer) and NA15OAR4310147 (Catherine Ivanovich and Radley M. Horton). Colin Raymond's portion of the work was carried out at the Jet Propulsion Laboratory, California Institute of Technology, under a contract with the National Aeronautics and Space Administration (80NM0018D0004).

References

Baldwin, J. W., Dessy, J. B., Vecchi, G. A., & Oppenheimer, M. (2019). Temporally compound heat wave events and global warming: An emerging hazard. *Earth's Future*, *7*(4), 411–427. https://doi.org/10.1029/2018ef000989

Borg, M. A., Xiang, J., Anikeeva, O., Pisaniello, D., Hansen, A., Zander, K., et al. (2021). Occupational heat stress and economic burden: A review of global evidence. *Environmental Research*, *195*, 1–14. https://doi.org/10.1016/j.envres.2021.110781

Buzan, J. R., & Huber, M. (2020). Moist heat stress on a hotter Earth. *Annual Review of Earth and Planetary Sciences*, *48*, 623–655. https://doi.org/10.1146/annurev-earth-053018-060100

Buzan, J. R., Oleson, K., & Huber, M. (2015). Implementation and comparison of a suite of heat stress metrics within the Community Land Model version 4.5. *Geoscientific Model Development*, *8*(2), 151–170. https://doi.org/10.5194/gmd-8-151-2015

Chen, D., Rojas, M., Samset, B. H., Cobb, K., Diongue Niang, A., Edwards, P., et al. (2021). Framing, context, and methods. In V. Masson-Delmotte, P. Zhai, A. Pirani, S. L. Connors, C. Péan, S. Berger, et al. (Eds.), *Climate change 2021: The physical science basis. Contribution of Working Group I to the Sixth Assessment Report of the Intergovernmental Panel on Climate Change*. Cambridge University Press.

Coffel, E. D., Horton, R. M., & de Sherbinin, A. (2018). Temperature and humidity based projections of a rapid rise in global heat stress exposure during the 21st century. *Environmental Research Letters*, *13*(1), 014001. https://doi.org/10.1088/1748-9326/aaa00e

Copernicus Climate Change Service (C3S). (2017). *ERA5: Fifth generation of ECMWF atmospheric reanalyses of the global climate*. Copernicus Climate Change Service Climate Data Store (CDS). Retrieved from https://cds.climate.copernicus.eu/cdsapp#!/home

Davies-Jones, R. (2008). An efficient and accurate method for computing the wet-bulb temperature along pseudoadiabats. *Monthly Weather Review*, *136*(7), 2764–2785. https://doi.org/10.1175/2007MWR2224.1

Di Napoli, C., Pappenberger, F., & Cloke, H. L. (2019). Verification of heat stress thresholds for a health-based heat-wave definition. *Journal of Applied Meteorology and Climatology*, *58*(6), 1177–1194. https://doi.org/10.1175/jamc-d-18-0246.1

Dunne, J. P., Stouffer, R. J., & John, J. G. (2013). Reductions in labour capacity from heat stress under climate warming. *Nature Climate Change*, *3*, 563–566. https://doi.org/10.1038/nclimate1827

Foster, J., Smallcombe, J. W., Hodder, S., Jay, O., Flouris, A. D., Nybo, L., & Havenith, G. (2021). An advanced empirical model for quantifying the impact of heat and climate change on human physical work capacity. *International Journal of Biometeorology*, *65*, 1215–1229. https://doi.org/10.1007/s00484-021-02105-0

Freychet, N., Tett, S. F. B., Yan, Z., & Li, Z. (2020). Underestimated change of wet-bulb temperatures over East and South China. *Geophysical Research Letters*, *47*(3), e2019GL086140. https://doi.org/10.1029/2019GL086140

Gagnon, D., & Crandall, C. G. (2018). Sweating as a heat loss thermoeffector. *Handbook of Clinical Neurology*, *156*, 211–232. https://doi.org/10.1016/B978-0-444-63912-7.00013-8

Goldie, J., Alexander, L., Lewis, S. C., & Sherwood, S. (2017). Comparative evaluation of human heat stress indices on selected hospital admissions in Sydney, Australia. *Australian & New Zealand Journal of Public Health*, *41*(4), 381–387. https://doi.org/10.1111/1753-6405.12692

Guirguis, K., Basu, R., Al-Delaimy, W. K., Benmarhnia, T., Clemesha, R. E. S., Corcos, I., et al. (2018). Heat, disparities, and health outcomes in San Diego County's diverse climate zones. *GeoHealth*, *2*(7), 212–223. https://doi.org/10.1029/2017gh000127

Gulev, S. K., Thorne, P. W., Ahn, J., Dentener, F. J., Domingues, C. M., Gerland, S., et al. (2021). Changing state of the climate system. In V. Masson-Delmotte, P. Zhai, A. Pirani, S. L. Connors, C. Péan, S. Berger, et al. (Eds.), *Climate change 2021: The physical science basis. Contribution of Working Group I to the Sixth Assessment Report of the Intergovernmental Panel on Climate Change*. Cambridge University Press.

Iturbide, M., Gutiérrez, J. M., Alves, L. M., Bedia, J., Cerezo-Mota, R., Cimadevilla, E., et al. (2020). An update of IPCC climate reference regions for subcontinental analysis of climate model data: Definition and aggregated datasets. *Earth System Science Data*, *12*(4), 2959–2970. https://doi.org/10.5194/essd-12-2959-2020

Jung, M., Reichstein, M., Ciais, P., Seneviratne, S. I., Sheffield, J., Goulden, M. L., et al. (2010). Recent decline in the global land evapotranspiration trend due to limited moisture supply. *Nature*, *467*, 951–954. https://doi.org/10.1038/nature09396

Kang, S., & Eltahir, E. A. B. (2018). North China Plain threatened by deadly heatwaves due to climate change and irrigation. *Nature Communications*, *9*, 2894. https://doi.org/10.1038/s41467-018-05252-y

Kjellstrom, T., Briggs, D., Freyberg, C., Lemke, B., Otto, M., & Hyatt, O. (2016). Heat, human performance, and occupational health: A key issue for the assessment of global climate change impacts. *Annual Review of Public Health*, *37*, 97–112. https://doi.org/10.1146/annurev-publhealth-032315-021740

Kopp, B. (2020). *WetBulb.m*. Retrieved from https://github.com/bobkopp/WetBulb.m

Krakauer, N. Y., Cook, B. I., & Puma, M. J. (2020). Effect of irrigation on humid heat extremes. *Environmental Research Letters*, *15*(9), 094010. https://doi.org/10.1088/1748-9326/ab9ecf

Li, C., Zhang, X., Zwiers, F., Fang, Y., & Michalak, A. M. (2017). Recent very hot summers in northern hemispheric land areas measured by wet bulb globe temperature will be the norm within 20 years. *Earth's Future*, *5*(12), 1203–1216. https://doi.org/10.1002/2017EF000639

Li, X.-X. (2020). Heat wave trends in Southeast Asia during 1979-2018: The impact of humidity. *Science of the Total Environment*, *721*, 137664. https://doi.org/10.1016/j.scitotenv.2020.137664

Limones, N., Marzo-Artigas, J., Wijnen, M., & Serrat-Capdevila, A. (2020). Evaluating drought risk in data-scarce contexts. The case of southern Angola. *Journal of Water and Climate Change*, *11*(S1), 44–67. https://doi.org/10.2166/wcc.2020.101

Liu, X., Tang, Q., Liu, W., Yang, H., Groisman, P., Leng, G., et al. (2019). The asymmetric impact of abundant preceding rainfall on heat stress in low latitudes. *Environmental Research Letters*, *14*, 044010. https://doi.org/10.1088/1748-9326/ab018a

Lo, M.-H., Wey, H.-W., Im, E.-S., Tang, L. I., Anderson, R. G., Wu, R.-J., et al. (2021). Intense agricultural irrigation induced contrasting precipitation changes in Saudi Arabia. *Environmental Research Letters*, *16*, 064049. https://doi.org/10.1088/1748-9326/ac002e

Margolis, H. G. (2014). Heat waves and rising temperatures: Human health impacts and the determinants of vulnerability. In K. E. Pinkerton, & W. N. Rom (Eds.), *Global climate change and public health. Respiratory medicine* (Vol. 7, pp. 85–120). https://doi.org/10.1007/978-1-4614-8417-2_6

Mishra, V., Ambika, A. K., Asoka, A., Aadhar, S., Buzan, J., Kumar, R., & Huber, M. (2020). Moist heat stress extremes in India enhanced by irrigation. *Nature Geoscience*, *13*, 722–728. https://doi.org/10.1038/s41561-020-00650-8

Monteiro, J. M., & Caballero, R. (2019). Characterization of extreme wet-bulb temperature events in southern Pakistan. *Geophysical Research Letters*, *46*(17–18), 10659–10668. https://doi.org/10.1029/2019GL084711

Mora, C., Dousset, B., Caldwell, I. R., Powell, F. E., Geronimo, R. C., Bielecki, C. R., et al. (2017). Global risk of deadly heat. *Nature Climate Change*, *7*, 501–506. https://doi.org/10.1038/nclimate3322

NOAA. (2021). *Cold & warm episodes by season*. Retrieved from https://origin.cpc.ncep.noaa.gov/products/analysis_monitoring/ensostuff/ONI_v5.php

Odnoletkova, N., & Patzek, T. W. (2021). Data-driven analysis of climate change in Saudi Arabia: Trends in temperature extremes and human comfort indicators. *Journal of Applied Meteorology and Climatology*, *60*(8), 1055–1070. https://doi.org/10.1175/JAMC-D-20-0273.1

Pal, J. S., & Eltahir, E. A. B. (2016). Future temperature in southwest Asia projected to exceed a threshold for human adaptability. *Nature Climate Change*, *6*, 197–200. https://doi.org/10.1038/nclimate2833

Ranasinghe, R., Ruane, A. C., Vautard, R., Arnell, N., Coppola, E., Cruz, F. A., et al. (2021). Climate change information for regional impact and for risk assessment. In V. Masson-Delmotte, P. Zhai, A. Pirani, S. L. Connors, C. Péan, S. Berger, et al. (Eds.), *Climate change 2021: The physical science basis. Contribution of Working Group I to the Sixth Assessment Report of the Intergovernmental Panel on Climate Change*. Cambridge University Press.

Raymond, C., Matthews, T., & Horton, R. M. (2020). The emergence of heat and humidity too severe for human tolerance. *Science Advances*, *6*(19). https://doi.org/10.1126/sciadv.aaw1838

Rogers, C. D. W., Ting, M., Li, C., Kornhuber, K., Coffel, E. D., Horton, R. M., et al. (2021). Recent increases in exposure to extreme humid-heat events disproportionately affect populated regions. *Geophysical Research Letters*, *48*(19), e2021GL094183. https://doi.org/10.1029/2021GL094183

Sathaye, J. A., Dale, L. L., Larsen, P. H., Fitts, G. A., Koy, K., Lewis, S. M., & de Lucena, A. F. P. (2013). Estimating impacts of warming temperatures on California's electricity system. *Global Environmental Change*, *23*(2), 499–511. https://doi.org/10.1016/j.gloenvcha.2012.12.005

Schröder, M., Lockhoff, M., Shi, L., August, T., Bennartz, R., Brogniez, H., et al. (2019). The GEWEX water vapor assessment: Overview and introduction to results and recommendations. *Remote Sensing*, *11*(3), 251. https://doi.org/10.3390/rs11030251

Sherwood, S. C., & Huber, M. (2010). An adaptability limit to climate change due to heat stress. *Proceedings of the National Academy of Sciences of the United States of America*, *107*(21), 9552–9555. https://doi.org/10.1073/pnas.0913352107

Spangler, K. R., & Wellenius, G. A. (2021). Spatial and intraseasonal variation in changing susceptibility to extreme heat in the United States. *Environmental Epidemiology*, *5*(2), e136. https://doi.org/10.1097/ee9.0000000000000136

Thiery, W., Visser, A. J., Fischer, E. M., Hauser, M., Hirsch, A. L., Lawrence, D. M., et al. (2020). Warming of hot extremes alleviated by expanding irrigation. *Nature Communications*, *11*, 290. https://doi.org/10.1038/s41467-019-14075-4

United Nations Assistance Mission in Afghanistan. (2016). *Water rights: An assessment of Afghanistan's legal framework governing water for agriculture*. Retrieved from https://unama.unmissions.org/sites/default/files/2016_19_10_water_rights_final_v2.pdf

Vanos, J. K., & Grundstein, A. J. (2020). Variations in athlete heat-loss potential between hot-dry and warm-humid environments at equivalent wet-bulb globe temperature thresholds. *Journal of Athletic Training*, *55*(11), 1190–1198. https://doi.org/10.4085/1062-6050-313-19

Vecellio, D. J., Wolf, S. T., Cottle, R. M., & Kenney, W. L. (2022). Evaluating the 35°C wet-bulb temperature adaptability threshold for young, healthy subjects (PSU HEAT Project). *Journal of Applied Physiology*, *132*(2), 340–345. https://doi.org/10.1152/japplphysiol.00738.2021

Vicente-Serrano, S. M., Nieto, R., Gimeno, L., Azorin-Molina, C., Drumond, A., El Kenawy, A., et al. (2018). Recent changes of relative humidity: Regional connections with land and ocean processes. *Earth System Dynamics*, *9*(2), 915–937. https://doi.org/10.5194/esd-9-915-2018

Willett, K. M., & Sherwood, S. (2012). Exceedance of heat index thresholds for 15 regions under a warming climate using the wet-bulb globe temperature. *International Journal of Climatology*, *32*(2), 161–177. https://doi.org/10.1002/joc.2257

WMO. (2020). *Climate explorer results: Effects of El Niño and La Niña on world weather*. Retrieved from https://climexp.knmi.nl/effects.cgi

Zander, K. K., Botzen, W. J. W., Oppermann, E., Kjellstrom, T., & Garnett, S. T. (2015). Heat stress causes substantial labour productivity loss in Australia. *Nature Climate Change*, *5*, 647–651. https://doi.org/10.1038/nclimate2623